

Waste-recycling Monte Carlo with optimal estimates: application to free energy calculations in alloys.

Gilles Adjanor

Groupe Métallurgie, MMC, EDF, Les Renardières, 77818 Moret-sur-Loing, France

Manuel Athènes

CEA, DEN, Service de Recherches de Métallurgie Physique, 91191 Gif-sur-Yvette, France

Jocelyn M. Rodgers

Physical Biosciences Division, Lawrence Berkeley National Laboratory Berkeley, CA 94720, USA

The estimator proposed recently by Delmas and Jourdain for waste-recycling Monte Carlo achieves variance reduction optimally with respect to a control variate that is evaluated directly using the simulation data. Here, the performance of this estimator is assessed numerically for free energy calculations in generic binary alloys and compared to those of other estimators taken from the literature. A systematic investigation with varying simulation parameters of a simplified system, the anti-ferromagnetic Ising model, is first carried out in the transmutation ensemble using path-sampling. We observe numerically that (i) the variance of the Delmas-Jourdain estimator is indeed reduced compared to that of other estimators; and that (ii) the resulting reduction is close to the maximal possible one, despite the inaccuracy in the estimated control variate. More extensive path-sampling simulations involving a FeCr alloy system described by a many-body potential additionally show that (iii) gradual transmutions accommodate the atomic frustrations, thus alleviating the numerical ergodicity issue present in numerous alloy systems and eventually enabling the determination of phase coexistence conditions.

I. INTRODUCTION

In Monte Carlo simulations of multi-particle systems, thermodynamic quantities are traditionally estimated by an arithmetic mean taken over the Markov chain of states constructed by the simulation. As a result, the information pertaining to the trial states that have been generated and rejected by the Metropolis-Hasting algorithm is lost. In contrast, waste-recycling Monte Carlo is a technique which includes this information in the estimate in order to improve its accuracy.¹

Waste-recycling estimators have been provided for quantum Monte Carlo schemes,² multi-proposal algorithms,³ parallel tempering (with pair-replica exchanges⁴ or multiple-replica exchanges⁵), path-sampling^{6,7} and path-sampling with multi-proposal.⁸⁻¹¹ In most implementations, waste-recycling was shown to be beneficial for estimating free energies or potentials of mean force, in the sense that variance reduction was observed numerically. Cases of variance augmentation have however been reported,^{11,12} showing that the additional recycled information is not always relevant.

Nevertheless, Delmas and Jourdain demonstrated mathematically that variance reduction is indeed achieved in the asymptotic limit when the acceptance function is symmetric to the identity of the old and the proposed state, as is the case for the sampling algorithm named after Boltzmann, Glauber or Barker. The estimator including information from both the old and the proposed state is then the associated conditional expectation.¹³ The authors also cast waste-recycling Monte Carlo into a general control variate problem structure and derived the optimal choice of the control variate in terms of asymptotic variance.

The purpose of this article is to investigate the relevance of the optimal estimator for calculating free energy differences, a crucial task of molecular simulation.¹⁴ The article is organized as follows. The multi-particle system is presented formally in Sec. II along with a broader overview of the weighted path ensemble approach employed, while the more specific aspects concerning the simulated binary alloys are deferred until Sec. V. Weighted path ensemble averages are derived in Sec. III and the Monte Carlo algorithm, including the mono-proposal sampling scheme and various estimators, are described in Sec. IV. In Sec. V, the methodology is applied to the calculation of chemical potential differences in binary alloys. While the primary goal of the study is to compare the statistical variance of the Delmas-Jourdain estimator with that of other estimators, we also illustrate the possibilities of the methodology by determining coexistence conditions using the equal-area construction on the chemical potential surface or the common-tangent construction on the reconstructed Gibbs free energy surface.

II. EXTENDED SYSTEM AND DYNAMICS

In this article we are interested in calculating the free energy difference for converting one particle of an alloy from one component type to the other, the systems 0 and 1 discussed below. In order to achieve this, we will employ extended systems which allow us to convert the Hamiltonian of the system of one composition to the Hamiltonian of the system of the other composition via a switching parameter λ , in a manner reminiscent of thermodynamic integration or nonequilibrium work calculations. In this section, we introduce much of the basic notation and terminology, and in the subsequent section, we discuss how the statistical physics of these paths generated while switching λ may be used to construct an alternate work-weighted path ensemble which is particularly well-posed for transmutations between differing alloy compositions.

The free energy of a multi-particle system of interest, labeled 1, can only be computed as a difference with respect to a reference thermodynamic state labeled 0. Let $H_1(x)$ and $H_0(x)$ denote the Hamiltonians of the respective systems with $x \equiv (q, p)$ denoting the particle positions q and the particle momenta p composing phase space. We define an extended Hamiltonian $H(\chi) = (1 - \lambda)H_0(x) + \lambda H_1(x)$ for $0 \leq \lambda \leq 1$ with respect to the extended state $\chi = (\lambda, x)$. The switching parameter λ is considered as an additional coordinate for the sake of generality, as the extended Hamiltonian can be given more general forms. The phase space associated with all extended states χ such that $\lambda = \alpha$ is denoted ω_α , and the union $\omega = \cup_{0 \leq \lambda \leq 1} \omega_\lambda$ defines the extended phase space. The probability densities in ω_α and ω are written respectively as

$$\begin{aligned} \rho_\alpha(\chi) &= \delta_{\lambda-\alpha}(\chi) \exp[\beta(G_\alpha - H_\alpha(x))] \\ \rho(\chi) &= \exp[\beta(G - H(\chi))] \end{aligned} \quad (1)$$

where G_α and G are the Gibbs free energy of the particle system and of the extended system, respectively, and the inverse temperature is β . The pressure P and volume V are implicitly accounted for by the Hamiltonian. The delta measure $\delta_{\lambda-\alpha}(d\chi) \equiv \delta_{\lambda-\alpha}(\chi)d\chi$ is such that under Lebesgue integration $\int_\omega \varphi(\lambda)\delta_{\lambda-\alpha}(d\chi) = \varphi(\alpha)$ for any test function φ .¹⁵ The Gibbs free energies G_α and G are related to each other via the identity

$$G_\alpha = G - \beta^{-1} \ln \int_{\omega_\alpha} \rho(\chi) d\chi. \quad (3)$$

In the following, the switching parameter will continuously evolve between states 0 and 1, but the two values of α of interest for calculating thermodynamic values will be 0 and 1. The thermodynamical expectation of quantity ϕ is expressed as

$$\langle \rho_\alpha, \phi \rangle = \int \phi(x) \rho_\alpha(\chi) d\chi. \quad (4)$$

Equation (4) will be estimated using a waste-recycling Monte Carlo technique from Ref. 11 with appropriate modifications to reflect the recently developed Delmas-Jourdain optimal estimator. To improve ergodicity in the phase space as well as the accuracy of the estimates, the trial moves are trajectories generated within a path ensemble using Langevin dynamics at temperature β^{-1} and constant pressure P , yielded by coupling the particles to a thermostat and barostat. In addition, an external force $f_\lambda^{\text{ext}}(x, \lambda)$ depending on the extended state acts upon the additional variable λ mechanically. In the most general set-up, λ is equipped with a mass m_λ and evolves according to

$$m_\lambda \ddot{\lambda} = f_\lambda^{\text{ext}} - \partial_\lambda H(x, \lambda), \quad (5)$$

assuming that λ is not restricted to the $[0,1]$ interval. A path $z = \{\chi_t\}_{0 \leq t \leq \tau}$ of duration τ consists of the sequence of the states $\chi_{0 \leq t \leq \tau}$ generated by the Langevin dynamics starting from χ_0 . The conditional probability to generate path z knowing the initial state χ_0 of the system is denoted by $P_{\text{fwd}}(\chi_{0 \leq t \leq \tau} | \chi_0)$ and can be evaluated numerically from the normal random deviates used in the stochastic dynamics. The reverse of path z is denoted by $z^\dagger = \{\chi_t^\dagger\}_{0 \leq t \leq \tau}$ and $\chi_t^\dagger = (\lambda, q, -p)_{\tau-t}$ where $(\lambda, q, p)_t = \chi_t$. The conditional probability to generate path z backward knowing the final state χ_τ of the system is the probability to generate z^\dagger forward from χ_0^\dagger

$$P_{\text{rev}}(\chi_{0 \leq t \leq \tau} | \chi_\tau) = P_{\text{fwd}}(\chi_{0^\dagger \leq t \leq \tau} | \chi_0^\dagger). \quad (6)$$

and is also evaluable from the normal deviates required to generate z^\dagger . In the following, the labeling of the probabilities with fwd and rev is dropped and we rather write

$$P(z | \chi_{\alpha\tau}) = P_{\text{rev}}(\chi_{0 \leq t \leq \alpha\tau} | \chi_{\alpha\tau}) P_{\text{fwd}}(\chi_{\alpha\tau \leq t \leq \tau} | \chi_{\alpha\tau})$$

The two values of α of interest will be 0 and 1. Hence, the nature of the probabilities is implied by the conditional presence of χ_0 or χ_τ .

The forward and reverse conditional probabilities above are two crucial quantities in waste-recycling Monte Carlo as their ratio enters the acceptance rule used both by the sampler (Sec. IV A) and the estimator (Sec. IV B). The ratio is related to the heat $Q(z)$ transferred from the thermostat and barostat into the system along z via the well-known expression^{16,17}

$$\frac{P(z|\chi_\tau)}{P(z|\chi_0)} = \exp[\beta Q(z)]. \quad (7)$$

In presence of an external force acting upon λ , the heat may be expressed as (see Eq. 26 and Eq. 27 in Ref. 10):

$$Q(z) = H(\chi_\tau) - H(\chi_0) - \int_{\lambda(0)}^{\lambda(\tau)} f_\lambda^{\text{ext}}(\chi_t) \dot{\lambda}(t) dt. \quad (8)$$

The integral of the product of the external force acting upon λ by the displacement $d\lambda = \dot{\lambda}dt$ corresponds to the mechanical work $W(z)$ done on the extended system. As a result, the identity in Eq. (7) can be cast into the equivalent form

$$\frac{P(z|\chi_\tau) \exp[-\beta H(\chi_\tau)]}{P(z|\chi_0) \exp[-\beta H(\chi_0)]} = \exp[-\beta W(z)]. \quad (9)$$

that will prove convenient for waste-recycling Monte Carlo because it contains the Hamiltonians of the distribution(s) of interest. Note that the identities in Eq. (7) or Eq. (9) remain valid when the evolution equation Eq. (5) is coupled to a thermal bath via an Ornstein-Uhlenbeck process.¹⁰

An autonomous scheduling of the additional coordinates based on the general evolution equation Eq. (5) enables the dynamics to explore all regions of interest while equilibrium information is retrieved using the ratio in Eq. (9) by waste-recycling Monte Carlo. This approach is particularly relevant when free-energy is to be reconstructed in multiple dimensions, or when the additional coordinates are meta-variables.^{18,19} Meta-variables are associated with, for instance, a restraining harmonic spring acting upon a generalised or reaction coordinate and characterize the position of a pulling device added to the particle system. Although the additional device modifies the Hamiltonian of interest, its contribution to thermodynamic expectations can be canceled by taking the ensemble average directly in the extended ensemble¹⁰, defined as follows

$$\langle \rho, \phi \rangle = \int \phi(x) \rho(x) dx. \quad (10)$$

Meta-variables are most commonly employed when constructing the free energy along reaction coordinates via umbrella sampling, which in its usual implementation¹⁴ entails correcting for the sampling bias rather than resorting to a marginal expectation like Eq. (10).

Here, we are interested in thermodynamic states 0 and 1 and need not consider Eq. (10). We further simplify Eq. (5) by requiring that λ varies at constant velocity from $\lambda(0) = 0$ to $\lambda(\tau) = 1$, as advocated by Jarzynski.^{20,21} The external force satisfying the resulting constraint $\ddot{\lambda} = 0$ in Eq. (5) is such that $f_\lambda^{\text{ext}} = \partial_\lambda H$, hence the work done on the extended system is

$$W(z) = \int_0^\tau \partial_\lambda H(\lambda_t, x_t) \dot{\lambda}_t dt. \quad (11)$$

III. WORK-WEIGHTED PATH ENSEMBLE

In this section, we show how the extended systems of the previous section may be employed to construct the work-weighted path ensemble used in our simulations and sampled by waste-recycling Monte Carlo.

In the following, the full trajectory space Ω encompasses all paths that connect the ω_0 and ω_1 phase subspace as the additional coordinate λ varies monotonically from 0 at $t = 0$ to 1 at $t = \tau$. Besides, two parameters α and θ are employed which formally may adopt the full range of possible values from 0 to 1. The intent of each of the parameters is distinct however. As previously mentioned, α is meant to indicate the thermodynamic states that we are interested in probing, and as such the meaningful values of α are strictly 0 and 1. The other parameter θ is a weighting factor supplied in constructing the path ensemble, in a sense indicating for each trajectory the contribution

of the two possible generating positions $\chi_0 = (0, x_0)$ and $\chi_\tau = (1, x_\tau)$ to its associated probability. In the results, a full range of θ values will be explored, but $\theta = 0.5$ is often advantageous,⁶ allowing for a good overlap²² with the two work histograms that can be constructed when paths are generated either forward from the equilibrium distribution of system 0 or backward from the equilibrium distribution of system 1.

The generalized path ensemble has a weighted probability density P_θ for the generating parameter θ in Ω given as^{7,22}

$$P_\theta(z) = e^{g_\theta} \{P(z|\chi_0) \exp[-\beta H(\chi_0)]\}^{1-\theta} \{P(z|\chi_\tau) \exp[-\beta H(\chi_\tau)]\}^\theta \quad (12)$$

where the normalizing constant g_θ ensures that P_θ is a probability distribution

$$\int_{\Omega} P_\theta(z) \mathcal{D}z = 1. \quad (13)$$

In the following discussion, the notation $\chi_{\alpha\tau}$ characterizes the state of path z at $t = \alpha\tau$, allowing us to develop the very similar equations for the states of interest, χ_0 and χ_τ , with more compact notation. For the two particular values $\alpha \in \{0, 1\}$, Eq. (13) is equivalent to

$$e^{g_\alpha} \int_{\omega_\alpha} e^{-\beta H(\chi)} d\chi = 1 \quad (14)$$

which results from the simplification of Eq. (12) into $P_\alpha(z) = e^{g_\alpha} e^{-\beta H(\chi_{\alpha\tau})} P(z|\chi_{\alpha\tau})$ and from the normalization of the conditional probabilities

$$\int_{\Omega(\chi_{\alpha\tau})} P(z|\chi_{\alpha\tau}) \mathcal{D}z = 1 \quad (15)$$

in each subspace $\Omega(\chi_{\alpha\tau})$ consisting of paths going through $\chi_{\alpha\tau}$. As a result, the logarithm of Eq. (14) with $\alpha \in \{0, 1\}$ reads

$$g_\alpha = -\ln \int_{\omega_\alpha} \exp[-\beta H(\chi)] d\chi = \beta G_\alpha, \quad (16)$$

indicating that these normalization constants g_0 and g_1 are indeed free energies for the two endpoint systems.

The normalization of the conditional probabilities for $\alpha \in \{0, 1\}$ also enables one to express the thermodynamic expectation of any quantity ϕ with respect to the path density P_α rather than the state density ρ_α (for $\alpha = 0$ or 1)

$$\begin{aligned} \langle \rho_\alpha, \phi \rangle &= \int_{\omega_\alpha} \phi(x) \exp[\beta(G_\alpha - H(\chi))] d\chi \\ &= \int \left(\int_{\Omega} \delta_\chi(\chi_{\alpha\tau}) \phi(x) e^{g_\alpha - \beta H(\chi)} P_\alpha(z|\chi_{\alpha\tau}) \mathcal{D}z \right) d\chi \\ &= \int \phi(x_{\alpha\tau}) P_\alpha(z) \mathcal{D}z \\ &= \langle P_\alpha, \phi_\alpha \rangle \end{aligned}$$

where $z \rightarrow \phi_\alpha(z)$ is the path functional such that $\phi_\alpha(z) = \phi(x_{\alpha\tau})$.

Since importance-sampling is achieved with respect to the distribution P_θ with $0 \leq \theta \leq 1$, we should rather employ to the formal path-average

$$\langle \rho_\alpha, \phi \rangle = \langle P_\theta, \phi_\alpha P_\alpha / P_\theta \rangle. \quad (17)$$

The probability density ratio in Eq. (17) can be cast into the form

$$P_\alpha / P_\theta = e^{\beta(\theta - \alpha)W + g_\alpha - g_\theta}, \quad (18)$$

obtained after substituting α for θ in Eq. (12), dividing by Eq. (12) while leaving θ intact, and further utilizing the connection between the conditional probabilities and W as defined in Eq. (9). Furthermore, substituting $e^{g_\theta - g_\alpha}$ for ϕ and ϕ_α in both sides of Eq. (17) yields

$$e^{g_\theta - g_\alpha} = \left\langle P_\theta, e^{\beta(\theta - \alpha)W} \right\rangle. \quad (19)$$

The form of Eq. (19) enables one to express Eq. (18) without the unknown normalizing constants g_α and g_θ , as follows

$$P_\alpha/P_\theta = e^{\beta(\theta-\alpha)\beta W} / \langle P_\theta, e^{\beta(\theta-\alpha)W} \rangle. \quad (20)$$

Inserting the probability ratio in Eq. (20) into the path average of Eq. (17) finally yields for $\alpha \in \{0, 1\}$

$$\langle \rho_\alpha, \phi \rangle = \langle P_\theta, \phi_\alpha e^{\beta(\theta-\alpha)W} \rangle / \langle P_\theta, e^{\beta(\theta-\alpha)W} \rangle. \quad (21)$$

The ratio involves two computationally tractable forms that can be estimated using Markov chain Monte Carlo methods. In particular, the free energy difference $G_1 - G_0 = \beta^{-1}(g_1 - g_0)$ can be obtained from the relationship

$$G_1 - G_0 = -\beta^{-1} \ln \frac{\langle P_\theta, \exp[\beta(\theta - 1)W] \rangle}{\langle P_\theta, \exp[\beta\theta W] \rangle}. \quad (22)$$

The effect of the bridging parameter θ on the numerical performance is discussed in Refs. 7 and 22 and further studied in Sec. V. Note that other work-biased distributions than P_θ and other ensemble averages have been proposed in the literature^{23,24} and are reviewed in Ref. 25. Here, one recovers Jarzynski's identity by choosing the importance function P_θ to be P_0

$$G_1 - G_0 = -\beta^{-1} \ln \langle P_0, \exp[-\beta W] \rangle. \quad (23)$$

Similarly, Crooks's probability ratio¹⁷

$$\frac{P(z|\chi_\tau)\rho_1(\chi_\tau)}{P(z|\chi_0)\rho_0(\chi_0)} = \exp[\beta(G_1 - G_0 - W(z))]. \quad (24)$$

is recovered from Eq. (20) after setting $\theta = 0$ and $\alpha = 1$ and then substituting $P\rho_0$ and $P\rho_1$ for P_0 and P_1 respectively. Equation (24) and Equation (9) are two mathematically equivalent identities referring to two distinct physical frameworks. In Eq. (24), $W(z)$ is to be interpreted as a nonequilibrium thermodynamic work, defined as the integral of the energies $\delta E(\lambda; x) = H(\lambda + \delta\lambda, x) - H(\lambda, x)$ transferred to the system as accounted for by small changes $\delta\lambda$ in the external generalized mechanical constraint λ .^{26,27} Constraining the system via the control parameter λ amounts to specifying the equilibrium distribution ρ_λ .

Within this framework, the identity in Eq. (24) entails a free energy difference. In contrast, with the physical prescription of Sec. II, the external mechanical force f_λ^{ext} acts transiently on λ for a duration τ and is then switched off. As a result, the system returns to its equilibrium distribution $\rho(\chi) = \exp[G - \beta H(\chi)]$. In this alternative framework,²⁶ the reverse and forward occurrence probabilities of path z in the ratio in Eq. (9) rather corresponds to a Bochkov-Kuzovlev identity.^{28,29}

Neither of the two above frameworks holds with respect to the weighted path ensembles with distributions P_θ when $0 < \theta < 1$ because, in this situation, no Hamiltonian-based equilibrium distribution can be defined for the state ensemble. The path formalism is merely introduced to facilitate the exploration of the phase space as will be shown in Sec. V. We now discuss how to sample P_θ and to estimate $\langle P_\theta, \cdot \rangle$ via a Markov chain Monte Carlo algorithm.

IV. WASTE-RECYCLING MONTE CARLO WITH MARKOV WEBS

A. Samplers

In practice, the distribution P_θ is approximated by a Markov chain constructed by importance sampling. Any sampler consists of two steps: (i) starting from a given path z_k , a trial path \tilde{z}_k is generated from a probability distribution q ; (ii) the trial path is accepted and added to the Markov chain $z_{k+1} = \tilde{z}_k$ with an adequate probability p , otherwise $z_{k+1} = z_k$. So as to ensure the convergence of the Markov chain towards the correct distribution, the transition probability matrix P must satisfy the following detailed balance equation

$$P(z_s, z)P_\theta(z) = P(z, z_s)P_\theta(z_s), \quad (25)$$

where $P(z_s, z)$ is the probability to transit from path z to path z_s , and vice versa for $P(z, z_s)$.

To formalize the sampler, we write the probability to construct the proposal \tilde{z} from z as $q(\{z, \tilde{z}\}|z)$ and the acceptance probability of the proposal as $p(\tilde{z}, \{z, \tilde{z}\})$, making the set of the proposed path and the original path

explicit in each case. The rejection probability is $1 - p(\tilde{z}, \{z, \tilde{z}\})$ and amounts to transiting to z . The transition probability from z to z_s is therefore¹³

$$P(z_s, z) = \sum_{\tilde{z}} [\delta_{\tilde{z}}(z_s) p(\tilde{z}, \{z, \tilde{z}\}) + \delta_z(z_s) (1 - p(\tilde{z}, \{z, \tilde{z}\}))] q(\{z, \tilde{z}\}|z), \quad (26)$$

where δ is the delta distribution and we allow for the possibility that z_s is either the old path z or the proposed path \tilde{z} . We write $q(\{z, \tilde{z}\}|\tilde{z})$ to express the backward probability enabling one to construct the current path z from the proposal \tilde{z} . Then, an acceptance probability that can be constructed from Eq. (25) and Eq. (26) is

$$p^M(\tilde{z}, \{z, \tilde{z}\}) = \min \left(1, \frac{q(\{z, \tilde{z}\}|\tilde{z}) P_\theta(\tilde{z})}{q(\{\tilde{z}, z\}|z) P_\theta(z)} \right). \quad (27)$$

This rule, proposed by Metropolis, is traditionally used because it maximizes the probability of acceptance. In particular, it is always larger than the acceptance probability of the Barker algorithm given by

$$p^B(\tilde{z}|\{z, \tilde{z}\}) = \frac{q(\{z, \tilde{z}\}|\tilde{z}) P_\theta(\tilde{z})}{q(\{z, \tilde{z}\}|\tilde{z}) P_\theta(\tilde{z}) + q(\{z, \tilde{z}\}|z) P_\theta(z)}. \quad (28)$$

This acceptance probability is symmetric so that $p^B(\tilde{z}|\{z, \tilde{z}\}) = p^B(\tilde{z}|\{\tilde{z}, z\})$, in contrast to the Metropolis rule p^M . Moreover, p^B appears to be a posterior likelihood associated with a marginal probability that is actually sampled by the algorithm (see Ref. 11 and Appendix A).

We consider that the sampler is such that the generated trial paths \tilde{z} share a common state $\chi_{\alpha\tau}$ with the current path z where $\alpha \in \{0, 1\}$. The constructed pairs of such paths are denoted by $\{z, \tilde{z}\}^\alpha$ and are called webs. The proposal functions are given by the conditional probabilities

$$q(\{z, \tilde{z}\}^\alpha|z) = r_\alpha P(\tilde{z}|\chi_{\alpha\tau}). \quad (29)$$

The factor r_α relates to the probability to choose $\alpha = 0$ or $\alpha = 1$. We similarly define $q(\{z, \tilde{z}\}^\alpha|\tilde{z}) = r_\alpha P(z|\chi_{\alpha\tau})$ for the reverse move, with the couple (r_0, r_1) in practice chosen to be alternately $(0, 1)$ and $(1, 0)$. Note that another possible choice consisting of setting $r_\alpha = \frac{1}{2}$ both for $\alpha = 0$ and $\alpha = 1$ appears less efficient numerically.¹¹

The Barker acceptance rule is therefore ($\alpha \in \{0, 1\}$)

$$p^B(\tilde{z}|\{z, \tilde{z}\}^\alpha) = \frac{\exp[\beta(\alpha - \theta)W(\tilde{z})]}{\exp[\beta(\alpha - \theta)W(z)] + \exp[\beta(\alpha - \theta)W(\tilde{z})]}. \quad (30)$$

Acceptance ratios for $0 < \alpha < 1$ are derived in the literature^{22,30} but are not implemented here.

Once the sampling process has been completed, the quantities of interest can be estimated from the constructed chain of webs $\{z_k, \tilde{z}_k\}_{1 \leq k \leq n}$.

B. Estimators

The standard estimator for the expectation $\langle P_\theta, f \rangle$ of a path functional f from a Markov chain of paths $\{z_k\}_{1 \leq k \leq n}$ distributed under P_θ is defined as

$$I_n(f) = \frac{1}{n} \sum_{k=1}^n f(z_k), \quad (31)$$

which is, in essence, the straightforward summation of states in the chain. In applications of Sec. V, the path functional f will be chosen to be $f = e^{\beta(\theta - \alpha)W}$.

Waste-recycling estimators are based on conditional expectations¹³ and include information from trial moves using the acceptance probability.^{1,2} In the path-ensemble, the waste-recycling estimator reads

$$I_n^{\text{WR}}(f) = \frac{1}{n} \sum_{k=1}^n f(z_k) p(z_k, \{z_k, \tilde{z}_k\}) + f(\tilde{z}_k) p(\tilde{z}_k, \{z_k, \tilde{z}_k\}) \quad (32)$$

where the nature of the webs indicating a shared state at either $\alpha = 0$ or $\alpha = 1$ is omitted for brevity and $\{z_k, \tilde{z}_k\}_{1 \leq k \leq n}$ is the web chain.

Following Delmas and Jourdain,¹³ waste-recycling is reformulated as a control variate problem consisting of searching the value $b \in \mathbb{R}$ minimizing the asymptotic variances $\sigma_\theta(f, bf)^2$ of the estimators $J_n^b(f)$ defined by

$$J_n^b(f) = (1 - b)I_n(f) + bI_n^{\text{WR}}(f). \quad (33)$$

Note that with the present notation, we have $J_n^0 = I_n$ and $J_n^1 = I_n^{\text{WR}}$ for the standard and waste-recycling estimators with respective asymptotic variances $\sigma_\theta(f, 0)^2$ and $\sigma_\theta(f, f)^2$. Delmas and Jourdain proved that the function $b \rightarrow \sigma_\theta(f, bf)^2 - \sigma_\theta(f, 0)^2$ is a convex quadratic form whose coefficients are easily evaluable when sampling is performed with the Barker algorithm. To make this remarkable feature of $\sigma_\theta(f, bf)^2$ clear, we shall write $\mathbb{E}_\theta[\varphi(z_1, z_0)]$ for the conditional expectation of function φ when z_0 is distributed under the invariant measure P_θ and z_1 is a random deviate constructed from z_0 using the sampler whose transition probability is $P(\cdot, z_0)$ given in Eq. (26).

The obtained quadratic form¹³

$$\sigma_\theta(f, bf)^2 - \sigma_\theta(f, 0)^2 = \frac{1}{2}\mathbb{E}_\theta \left[(f(z_1) - f(z_0))^2 \right] \times b^2 - 2 \{ \langle P_\theta, f^2 \rangle - \langle P_\theta, f \rangle^2 \} \times b \quad (34)$$

is valid for Barker sampling only. The coefficient of the first order term in b is the variance of the observable. The coefficient of the second order term is a conditional variance since $\mathbb{E}_\theta[f(z_1) - f(z_0)] = 0$ (we have $\langle P_\theta, f \rangle = \mathbb{E}_\theta[f(z_0)] = \mathbb{E}_\theta[f(z_1)]$). Since both variances are strictly positive for non-constant f on $\{z/P_\theta(z) > 0\}$, the quadratic form Eq. (34) has a minimum occurring at the strictly positive value

$$b^* = \frac{\langle P_\theta, f^2 \rangle - \langle P_\theta, f \rangle^2}{\frac{1}{2}\mathbb{E}_\theta \left[(f(z_1) - f(z_0))^2 \right]}. \quad (35)$$

It is moreover proven¹³ that $b^* > 1$ when $\sigma(f, f)^2 > 0$. To simplify the notation, the dependence of b^* on θ and f is omitted.

This implies that the value b^* that minimizes the variance can be estimated from a single run in spite of the fact the variance $\sigma_\theta(f, 0)^2$ of the standard estimator can only be evaluated from a sample of estimates $I_n(f)$ taken in the limit of large n owing to the central limit theorem.³¹ The optimal parameter b^* defined by Eq. (35) can be estimated by

$$\mathcal{I}_n(b^*) = \frac{I_n(f^2) - I_n(f)^2}{\frac{1}{2n} \sum_{k=1}^n (f(z_{k+1}) - f(z_k))^2}. \quad (36)$$

from the Markov chain. An alternative procedure to estimate the optimal parameter Eq. (35) consists of including information about trial paths \tilde{z}_k . In particular, $\mathbb{E}_\theta[\phi(z_1, z_0)]$ can be estimated via waste recycling by $\frac{1}{n} \sum_{k=1}^n p^B(\tilde{z}_k | \{z_k, \tilde{z}_k\})\phi(\tilde{z}_k, z_k) + p(z_k | \{z_k, \tilde{z}_k\})\phi(z_k, z_k)$. With $\phi(z_1, z_0) = (f(z_1) - f(z_0))^2$, the optimal parameter b^* defined by Eq. (35) can be estimated using

$$\mathcal{I}_n^{\text{WR}}(b^*) = \frac{I_n^{\text{WR}}(f^2) - I_n^{\text{WR}}(f)^2}{\frac{1}{2n} \sum_{k=1}^n p(\tilde{z}_k | \{z_k, \tilde{z}_k\})(f(\tilde{z}_k) - f(z_k))^2}. \quad (37)$$

Note that the waste-recycling estimator J_n^b is not optimal at b^* in terms of asymptotic variance when sampling is achieved with the Metropolis algorithm. The question whether one should resort to the optimal estimator and the suboptimal Barker sampler or to the optimal Metropolis sampler and a suboptimal estimator has not been answered theoretically and will be addressed numerically here.

V. APPLICATIONS

We now apply this waste recycling Monte Carlo on Markov webs to our system of interest, binary alloys of varying composition. Initially, we shall make clear how the general notation of the preceding sections is connected to this problem of interest. Subsequently, we delve in to the numerical applications. The performance of the optimal estimator is first assessed by comparing with that of traditional estimators in a generic but realistic binary system with A and B atoms interacting on a rigid lattice in Sec. V B. The possibilities of the methodology are then illustrated by performing off-lattice simulations of a model FeCr alloy in Sec. V C.

A. Binary alloys

The computational cell contains N atoms. In the reference state at $t = 0$, we have $N = N_A + N_B$ or $N = N_{\text{Fe}} + N_{\text{Cr}}$ atoms where N_X refers to the atom number of type X. In the target state at $t = \tau$, the cells still contains N atoms, but an A or Fe atom has been transmuted into a B or Cr atom, respectively. Paths thus consist of artificially switching the potential energy of a selected atom. The switching will be performed instantaneously in the AB alloy (Sec. VB), or gradually using constant-pressure Langevin dynamics²² in the FeCr alloy (Sec. VC).

The infinitely-fast transmutions of Sec. VB are carried out without changing the atomic masses. Hence, the ratio of the reverse conditional probability, $P(z|\chi_\tau) = (N_B + 1)^{-1}$, to the forward one, $P(z|\chi_0) = (N - N_B)^{-1}$, relates to the exponential of the ideal chemical potential difference

$$\frac{P(z|\chi_\tau)}{P(z|\chi_0)} = \frac{N_B + 1}{N - N_B} = \exp[\beta\Delta\mu^{\text{id}}]. \quad (38)$$

Plugging Eq. (38) into Eq. (9) leads to an identity relating the work W carried out on the system for transmuting an A atom into a B atom to the Hamiltonian variation

$$W(z) = H(\chi_\tau) - H(\chi_0) - \Delta\mu^{\text{id}} \quad (39)$$

where χ_τ only differs from χ_0 by the transmuted atom. When transmuting a B into an A atom, the quantity $-W(z)$ must be considered instead. Besides, $\Delta\mu^{\text{id}}$ acts as a heat transferred from a reservoir of A and B atoms into the system.

In contrast, the transmutions of Sec. VC are performed gradually using constant-pressure Langevin dynamics²² and linear Hamiltonian switching. As a result, the probability ratio Eq. (38) becomes

$$\frac{P(z|\chi_\tau)}{P(z|\chi_0)} = \exp[\beta\Delta\mu^{\text{id}} + \beta\mathcal{Q}(z)] \quad (40)$$

where $\mathcal{Q}(z)$ is the heat transferred from the thermostat and barostat to the particle system,²² in addition to the heat $\Delta\mu^{\text{id}}$ transferred from the atomic reservoir. We thus have

$$W(z) = H(\chi_\tau) - H(\chi_0) - \Delta\mu^{\text{id}} - \mathcal{Q}(z) \quad (41)$$

In both set-ups, sampling forward and backward transmutions is sufficient to explore the phase spaces of the alloy. As illustrated in Fig. 1, accepting several paths amounts to exchanging the allocation of atoms on the underlying lattice of the reference and target systems.

Simulations aim at extracting differences of chemical potentials $\Delta\mu$ between both species as a function of the alloy composition. We have either $\Delta\mu = \mu_B - \mu_A$ or $\Delta\mu = \mu_{\text{Cr}} - \mu_{\text{Fe}}$ depending on the involved alloy system. Both quantities indeed correspond to the difference of Gibbs free energy between the target and reference states

$$\Delta\mu = \beta^{-1}(g_1 - g_0). \quad (42)$$

The generic estimator will be

$$\mathcal{J}_n^b(\Delta\mu) = -\beta^{-1} \ln \frac{J_n^b(e^{\beta(\theta-1)W})}{J_n^b(e^{\beta\theta W})} \quad (43)$$

The numerator and denominator in the logarithm are estimates of $\exp[g_\theta - g_1]$ and $\exp[g_\theta - g_0]$ obtained simultaneously by sampling the probability measure P_θ and applying the generalized estimator in Eq. (33).

Let $c = N_B/N$ or $c = N_{\text{Cr}}/N$ denote the alloy concentration in B or Cr. A change in the monotonicity of the function $c \rightarrow \Delta\mu(c)$ is a signature of phase coexistence. The conditions of phase equilibria can then be determined via the equal-area construction with respect to $\Delta\mu(c)$, or equivalently, via the common-tangent construction with respect to the Gibbs free energy

$$G(c) = \int_0^c \Delta\mu(c')dc'. \quad (44)$$

measured per atom.

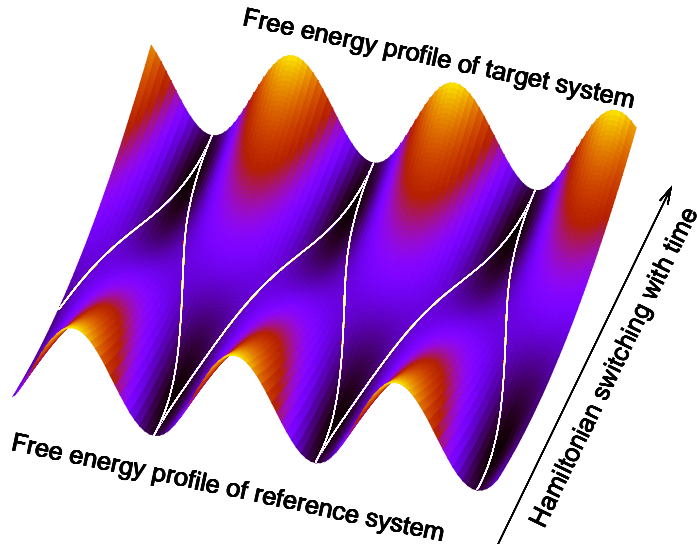


FIG. 1: Schematic free energy landscape in the extended space. The alloy undergoes forward and reverse atomic transmutations: white curves linking free energy minima symbolize the sampled transmutations. Path-sampling enables the simulation to explore the phase space of both the reference and target systems.

B. AB system with constant pair interactions

In our simplified binary alloy lattice model, the rigid lattice is body centered cubic. Interaction energies are taken as pair interactions ϵ_{XY} between nearest-neighbor sites, where X and Y may equal A or B. The ordering enthalpy $\epsilon = \epsilon_{AA} + \epsilon_{BB} - 2\epsilon_{AB}$ plays a key role as it entirely determines the thermodynamics of the system.³² Without loss of generality, we can choose $\epsilon_{AA} = \epsilon_{AB} = 0$ which leads to an Ising-type internal energy

$$H(\chi) = \epsilon \sum_{(i,j) \in E} \eta_B^i \eta_B^j \quad (45)$$

where the summation runs over the ensemble E of nearest neighbor pairs only and η_B^i is 1 or 0 depending on whether site i is occupied by a B atom or not. The cell contains $N = 2^{12}$ sites with N_B atoms of type B at $t = 0$.

We set $\epsilon = -30$ meV. With a negative ordering energy, the system exhibits a miscibility gap below which the solid solution decomposes into A-rich and B-rich phases. The unmixing transition is of first-order except for the $A_{0.5}B_{0.5}$ composition where it is second-order³² and where the critical temperature is $T_c \approx -\epsilon/(k \times 0.62)$.³³

We first check the Delmas-Jourdain prediction that the asymptotic variance $\sigma(f, bf)^2$ of $J_n^b(f)$ is minimal at $b = b^*$ when the Barker sampler is used. Since $\lim_{n \rightarrow +\infty} n \text{var}_n(f, bf) = \sigma(f, bf)^2$ where $\text{var}_n(f, bf)$ is the statistical variance of $J_n^b(f)$, we evaluate $\text{var}_n(f, bf)$ as a function of b for large enough n and confirm whether its minimum occurs close to estimated values of b^* . Note that $b \rightarrow \text{var}_n(f, bf)$ is a quadratic form regardless of the value of n .

We set temperature to 348 K, the simulation parameter θ to 1/2, and B concentration to 50at.%. The two quantities $\exp[g_{1/2} - g_0]$ and $\exp[g_{1/2} - g_1]$ are equal to each other for this particular set-up, and have been evaluated via ensemble average Eq. (19) and the estimator $J_n^b(f)$ given in Eq. (33) with $f = e^{\pm \frac{1}{2}\beta W}$ and $0 \leq b \leq 20$. The statistical variances $\text{var}_n(f, bf)$ have been computed from $m = 10^7$ estimates generated using distinct random seeds. Each estimate consists of $n = 2 \cdot 10^3$ transmutations, from A into B and from B into A alternatively. For each estimation, we also record the estimated value of b^* using estimator $\mathcal{I}_n(b^*)$ given in Eq. (36) and estimator $\mathcal{I}_n^{\text{WR}}(b^*)$ given in Eq. (37), and additionally construct their histograms: $\langle h^0(b - b^*) \rangle$ and $\langle h^1(b - b^*) \rangle$ respectively denote the probabilities that estimates $\mathcal{I}_n(b^*)$ or $\mathcal{I}_n^{\text{WR}}(b^*)$ are equal to b .

As shown in Fig. 2, the quadratic form $\text{var}_n(f, bf)$ is indeed minimum at the value corresponding to the best b^* -estimate indicated by the vertical double-dotted segment, obtained by combining the mn available data from either $\mathcal{I}_{nm}(b^*)$ or $\mathcal{I}_{nm}^{\text{WR}}(b^*)$. The minimum is also very close to the horizontal line labeled $\text{var}_n(f, fb_n^*)$ corresponding to a

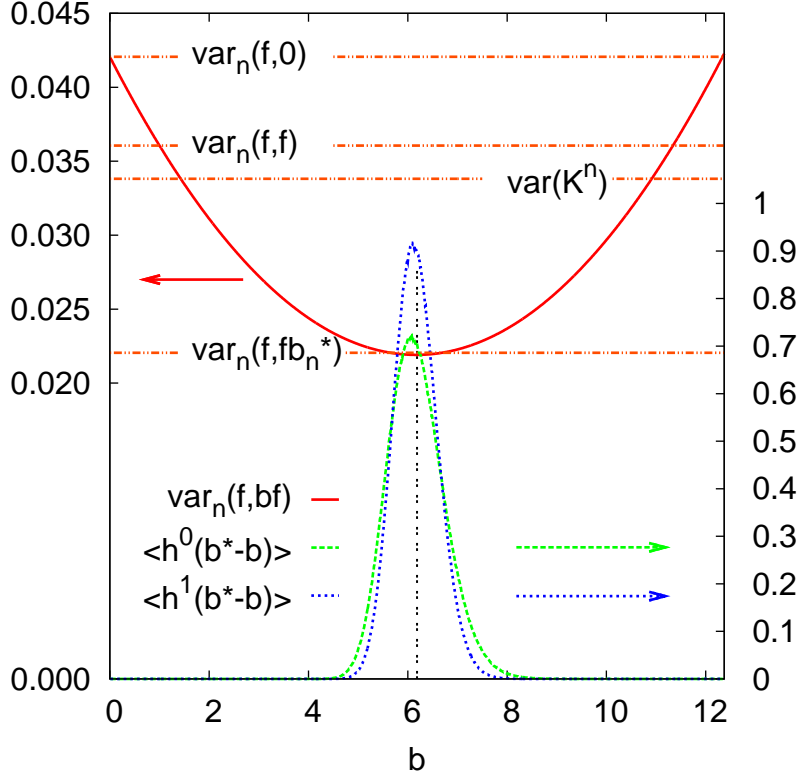


FIG. 2: (left ordinate) $\text{var}_n(f, bf)$ is the statistical variance of $J_n^b(e^{-\beta W/2})$ given in Eq. (33) and is evaluated from 10^7 estimates. Note that $\text{var}_n(f, 0)$ and $\text{var}_n(f, f)$ corresponds to the variances of $I_n(e^{-\beta W/2})$ and $I_n^{\text{WR}}(e^{-\beta W/2})$. $\text{var}_n(f, b_n^*)$ is defined in the text; (right ordinate) $\langle h^0(b^* - b) \rangle$ and $\langle h^1(b^* - b) \rangle$ are the histograms of optimal parameter b^* estimated without or with waste-recycling.

variance obtained from the m estimates $J_n^{b_n^*}(f)$ after substituting the corresponding $\mathcal{I}_n(b^*)$ for b_n^* in each estimate. Substituting $\mathcal{I}_n^{\text{WR}}(b^*)$ for b_n^* further decreases the variance by 0.24%, an amount not visible on the graph. A more noticeable benefit to employing waste-recycling for estimating b^* can be seen from the two histograms of b^* displayed in Fig. 2. Histogram $\langle h^1(b - b^*) \rangle$ is slightly narrower than histogram $\langle h^0(b - b^*) \rangle$ obtained without waste-recycling.

We also observe in Fig. 2 that the optimal estimator exhibits a smaller statistical variance than that of the residence-weight estimator K_n (derived in Appendix A), although the available theory does not predict the extent to which the observed tendency is general. We also don't know the value θ^* of the control parameter that minimizes the total variance in the estimates of $\Delta\mu$ from Eq. (43). Qualitatively, the symmetric setting $\theta = 1/2$ is often used^{6,7,22,30} because the work distribution associated with $P_{1/2}$ exhibits sufficient overlaps with those associated with both P_0 and P_1 , ensuring a fast convergence of the involved exponential averages.²²

We carried out a series of simulations with varying the value of θ in the range $[0, 1]$ so as to locate the optimal value θ^* with respect to the evaluation of $\Delta\mu$ using estimator Eq. (43), at the asymmetric composition $c = 10at.\%$ B. The statistical variance is obtained using $m = 10^7$ independent estimates but with $n = 2 \cdot 10^4$ transmutations in each estimate (10 times more than previously). The results in Fig. 3 demonstrate that the observed hierarchy in the estimator performance is preserved for any $\theta \in [0, 1]$. The optimal estimators $J_n^{b^*}$ achieve the best performance whether waste-recycling is used (h^1) or not (h^0) for estimating b^* . Interestingly, using the optimal estimator shifts the minimum of the variance to a value of θ close to 0.5 from a value about 0.7 with the standard estimator. Given that b^* is about 3 when $\theta = 1/2$ close to the minimum of the variance, the “standard” contribution involving the Markov chain of paths accepted in the sampled distribution P_θ is assigned with a weighting factor $1 - b^*$ close to the negative value of -2 . The “waste-recycling” contribution involves both the accepted and trial paths and is assigned with a weighting factor b^* that is positive and larger than $1 - b^*$ in absolute value. Hence, compared to the overall contribution of the accepted paths, trial transmutations generated from the forward and backward path distributions contribute to the free-energy estimates quite substantially.

We have then post-processed the collected data (the 10^7 estimates) by evaluating the statistical variances $\text{var}_n(f, bf)$ of estimator $J_n^b(f)$ (given in Eq. (33) with $f = e^{\beta(1/2-\alpha)W}$, $\alpha \in \{0, 1\}$ and $n = 2 \cdot 10^4$) as a function of $b \in [0, 20]$.

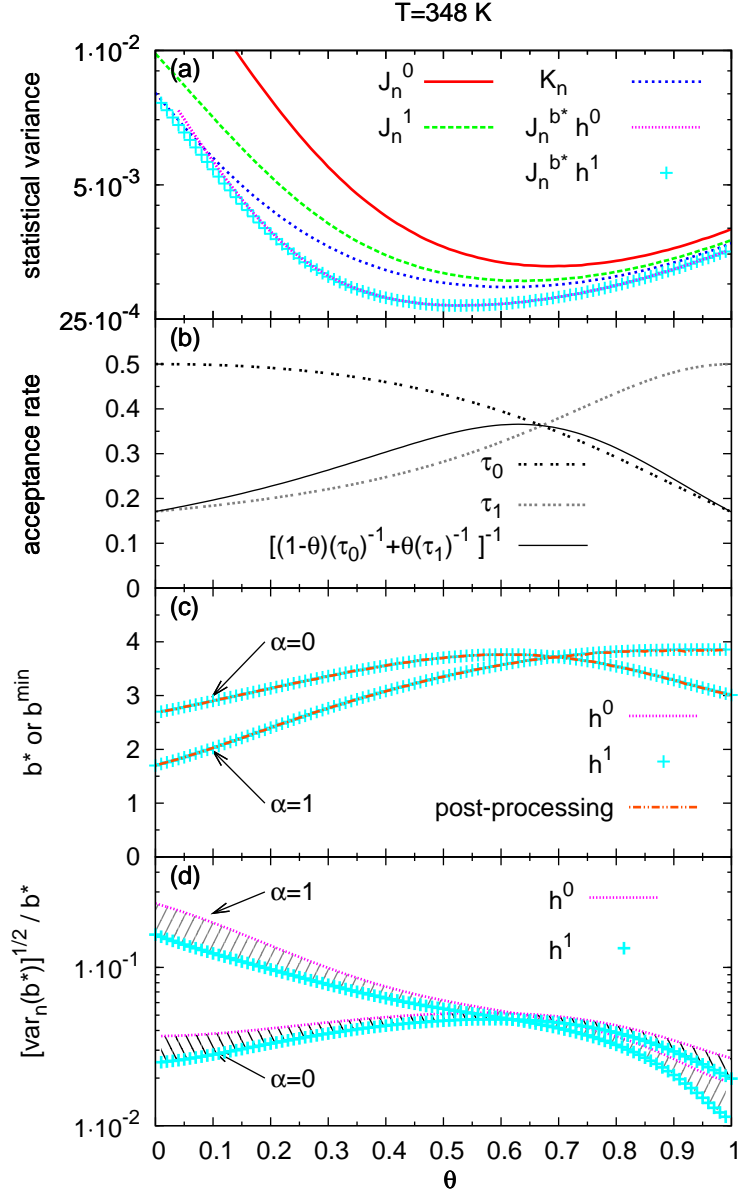


FIG. 3: (a) estimator variances; (b) acceptance rates; (c) optimal parameter; (d) reduced deviation of b^* as a function θ [$\text{var}_n(b^*)$ is the variance of the estimates of b^*]. Simulations are performed at $T = 348$ K.

The minima of the quadratic forms in b are plotted in panel (c) of Fig. 3 as a function of θ (curve labeled 'post-processing'). As expected theoretically, they perfectly coincide with the online estimations of b^* without waste recycling as in Eq. (36) or with waste recycling as in Eq. (37), which are also plotted for comparison. Panel (d) of Fig. 3 shows the higher accuracy obtained for the waste-recycling estimates via Eq. (37).

Additional simulations are carried out at temperature $\beta^{-1} = 174$ K with varying θ or at $\beta^{-1} = 348$ K with varying concentration (and imposing $\theta = 1/2$). Results are displayed in Fig. 4 and Fig. 5, respectively. The same qualitative trends are observed. Nonetheless, for the low temperature simulation, much smaller acceptance rates are measured. A small acceptance rate decreases the denominator in both Eq. (36) and Eq. (37) explaining the higher values of b^* and the difficulties in estimating the variance when $\theta < 0.25$ where a few negative estimates of $e^{g\theta - g\alpha}$ prevented

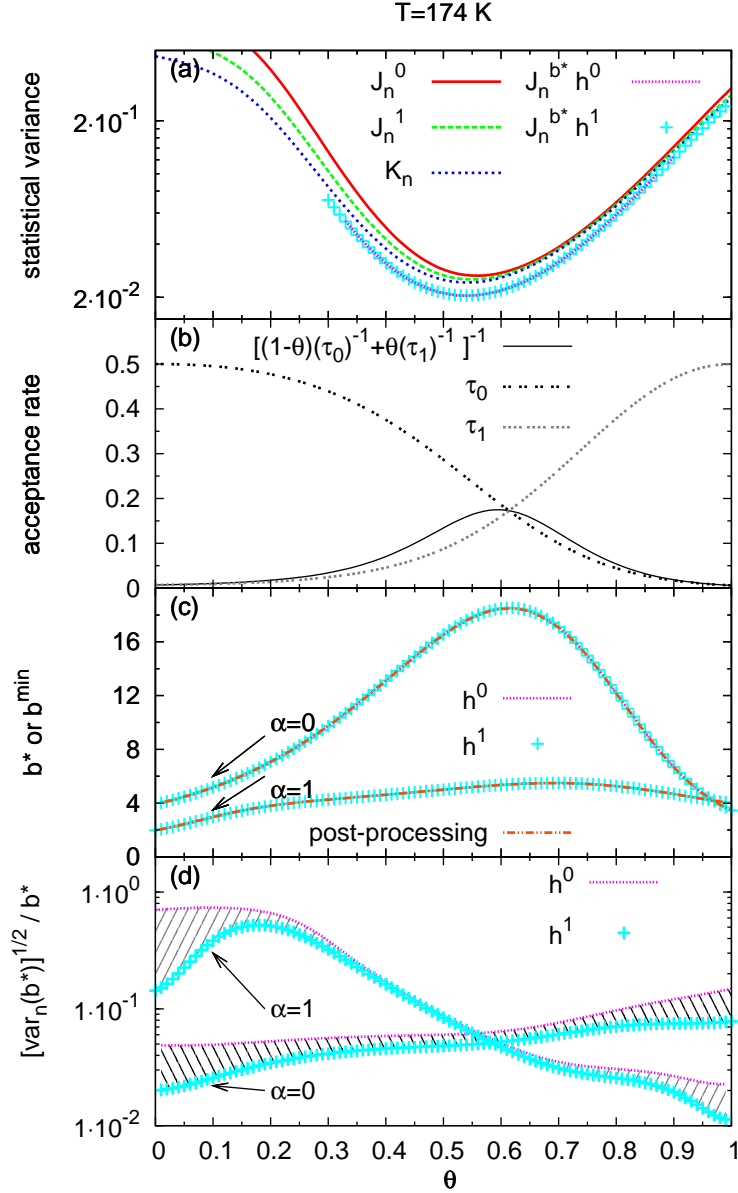


FIG. 4: Same as in Fig. 3 but at $T = 174$ K.

evaluation of the logarithm in Eq. (43).

We have carried out additional Monte Carlo simulations using the Metropolis sampler with $\theta = 0.5$ and $\beta^{-1} = 348$ K and with varying B concentration in order to compute the minima of the statistical variances of estimator $J_n^b(e^{\beta(1/2-\alpha)W})$ as a function of concentration and for $\alpha \in \{0, 1\}$. Similarly, 10^7 estimates have been used. The minima b^{\min} are plotted as a function of concentration in Fig. 5 (curve labeled 'post-processing') and do not coincide with the online estimation in Eq. (36) or Eq. (37), as expected for the Metropolis sampler.

Because evaluating statistical variances requires a considerable computational cost, accurately determining b^{\min} by post-processing from the minimum of the function $b \rightarrow \text{var}_n(f, bf)$ is more difficult than accurately estimating f , the quantity of interest. Post-processing the data obtained using the Metropolis sampler is thus not suitable to the simulation of realistic systems for which accuracy is an issue.

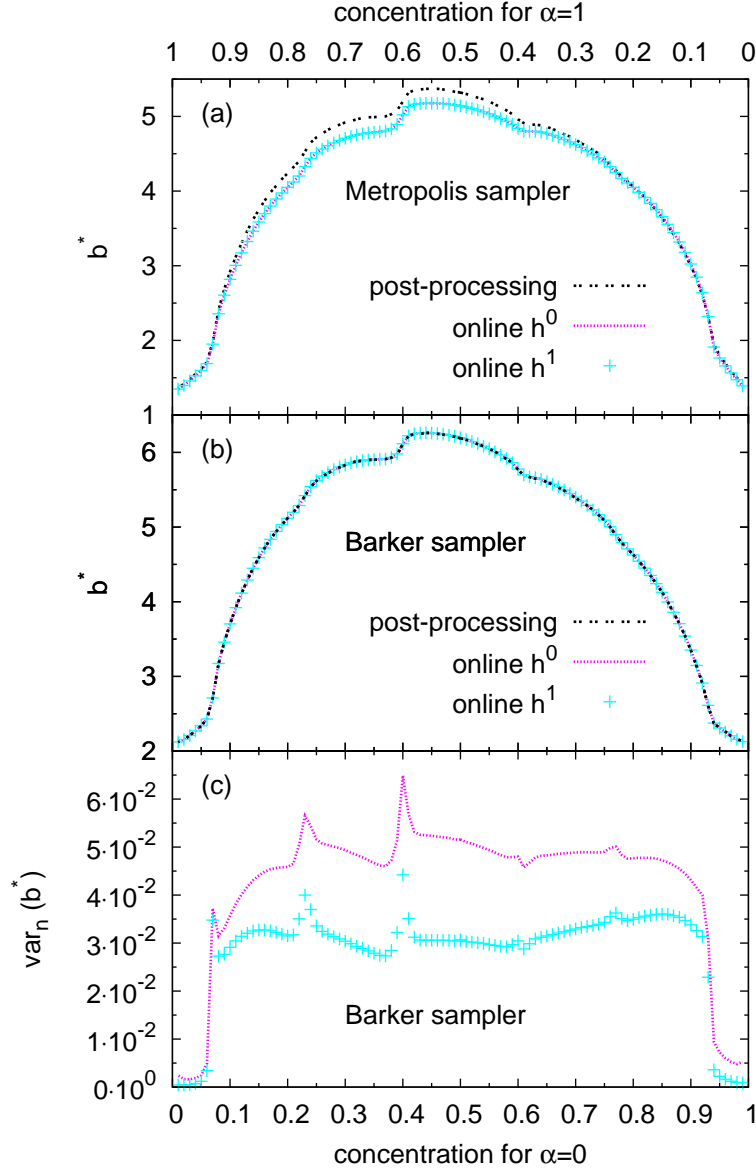


FIG. 5: (a) disagreement between b^* and b^{\min} obtained from the true minimum after post-processing with the Metropolis sampler; (b) agreement between the same quantities with the Barker sampler; (c) statistical variances of the b^* estimated with the Barker sampler.

The question of whether the combination of the optimal Metropolis sampler and the suboptimal estimators I_n or I_n^{WR} may achieve better efficiency than the combination of the suboptimal Barker sampler and the optimal estimator $J_n^{b^*}$ is not answered by theory.¹³ Therefore, we now address this numerically. The statistical variances of the $\Delta\mu$ -estimates obtained using the biased estimator of Eq. (43) have been calculated and plotted as a function of B concentration in Fig. 6. We observe that it is always more efficient to implement the optimized estimator $J_n^{b^*}$ with the suboptimal sampler than estimator J_n^1 with Metropolis sampling, or even the residence-weight estimator K_n with Metropolis sampling. Note that $J_n^{b^*}$ is still a valid and unbiased estimator when combined with the Metropolis sampler (but is not optimal anymore). Here, the combination was found slightly more efficient, with variance further decreased by 4.7% for $A_{0.5}B_{0.5}$ compared to Barker sampling and $J_n^{b^*}$. However, variance reduction is not guaranteed mathematically and cases of variance augmentations have been reported when implementing waste-recycling estimators with a Metropolis sampler.^{11,13}

Hence, the combination of Metropolis samplers with estimation of b is not recommended, is not presented in the plots, and is not further considered.

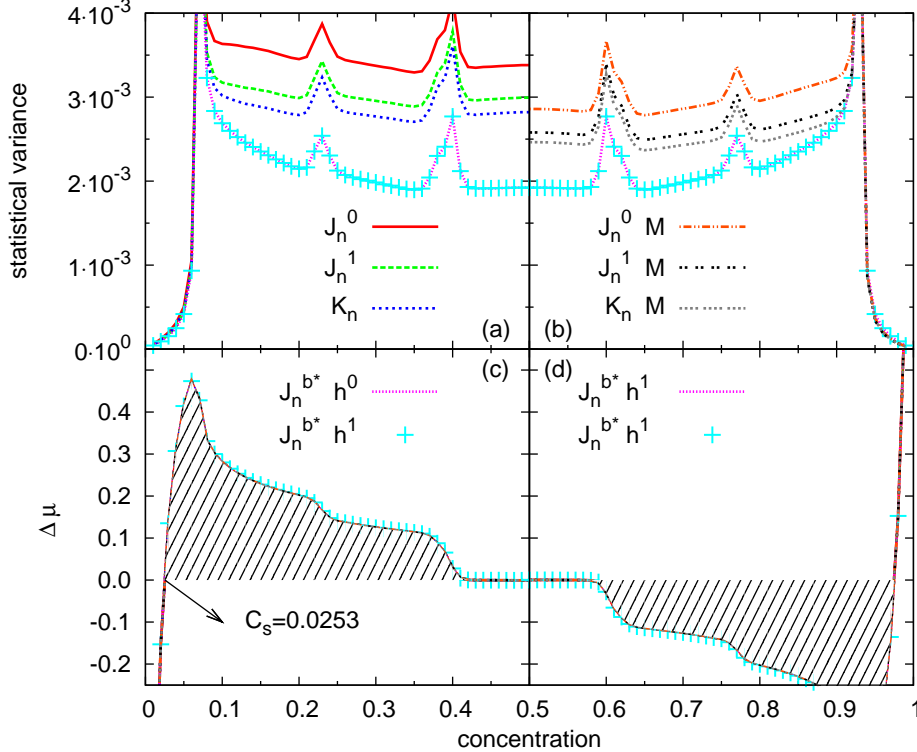


FIG. 6: (a,b) statistical variances of estimated differences of excess chemical potentials [displayed in (c,d)] as a function of concentration. Used estimators are indicated in the legends. The symmetry of this Ising system with respect to $C_B = 50\%$ explains the equality between chemical potentials ($\Delta\mu = 0$) at the solubility limit C_s .

C. Fe-Cr system with EAM interactions

We now test our estimators on a more difficult model whose inter-atomic potentials are based on the embedded atom method (EAM). We have implemented the EAM potentials of Olsson *et al.*³⁴ developed to model the α and α' phases of the FeCr binary system. While this EAM potential correctly reproduces the BCC structure of Iron and Chromium, its ground state (found among 99 candidate BCC structures based on the theory of the convex polyhedron in the correlation functions space³²) is an intermetallic structure with positive ordering enthalpy at $c=50$ at.% Cr.³⁵ So as to avoid the formation of additional phase stability fields, the intermetallic structure was excluded from the construction of the complete phase diagram using the Alloy-Theoretic Automated Toolkit (ATAT) package in Ref. 35. The ATAT approach involves, firstly, constructing effective cluster interaction energies on a rigid lattice based on a few relevant structures previously relaxed using the EAM potential and, secondly, performing Monte Carlo simulations on the rigid lattice. Note however that the expected miscibility gap of FeCr alloy was observed in Monte Carlo simulations carried out on a rigid lattice with the interaction energies directly deduced from the EAM potential.³⁴ Here, the rigid-lattice assumption is entirely released in the construction of the phase diagram.

We perform path-sampling simulations to compute the chemical potential difference with varying concentration and temperature. Transmutations are now performed gradually in 10^2 steps with linear Hamiltonian switching and constant-pressure Langevin dynamics²² in a computational cell containing 432 atoms. Equilibration proceeds in 20 transmutations per atom, starting from a random distribution of the atoms on 6^3 unit cells of the BCC structure. Simulations have been carried out with temperature ranging from 300 to 1700 K in step of 25 K. Examination of the simulated microstructures show evidence of phase separation at low enough temperatures. Figure 7 displays the snapshot of a typical phase separated microstructure for alloy $\text{Fe}_{0.8}\text{Cr}_{0.2}$ at 300 K.

Figure 8 displays the statistical variances obtained for the various estimators obtained with $n = 400$ transmutations (per estimate) and $m = 200$ estimates at $T=500$ K ($T = (k\beta)^{-1}$). The aforementioned hierarchy still holds in the present case for all concentrations. The Delmas-Jourdain estimator still achieves better efficiency than the residence-weight estimator. Because the amount of transmutations per estimate is much smaller than previously, it is more relevant to estimate b^* using waste-recycling (h^1) than without (h^0). The former variant further decreases the variance

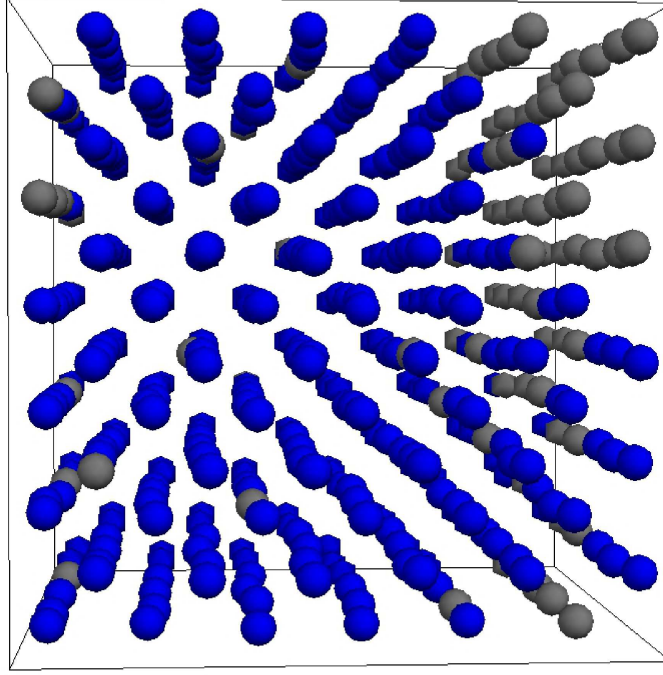


FIG. 7: Snapshot of a simulated microstructure containing 20% at. Cr obtained at $T = 300\text{K}$. Fe and Cr atoms are displayed in blue and gray, respectively.

associated with the estimation of b^* by 20 % on average over the latter one. Averaging over all temperatures, estimator $\mathcal{J}_n^{b^*} \cdot h^{-1}$ decreases the variance by a factor of 2 to 5/2 compared to \mathcal{J}_n^0 and by 20 to 30 % compared to $\mathcal{J}_n^{b^*}$ with h^0 . The $\Delta\mu$ -values displayed in Fig. 8b correspond to a single estimate obtained from the $8 \cdot 10^4 = m \times n$ transmutations used to evaluate the statistical variance. Figures 8b and 8c illustrate the equal-area or common-tangent constructions of Maxwell and corroborate the occurrence of phase coexistence.

The reconstructed Gibbs free energy surface G is less fluctuating because it is based on a self-averaging integral Eq. (44). The potential quantity $\Delta\mu^*(T)$ in Fig. 8c is such that the occurrence probabilities of the Fe-rich and Cr-rich phases are equal. The occurrence probability is $P^*(c, T) = Z^{-1} e^{N\beta[c\Delta\mu^* - G(c)]}$ where $Z = \int_0^1 e^{N\beta[c'\Delta\mu^* - G(c')]} dc'$ is the semigrand canonical partition function¹⁴ associated with the finite computational cell. The potential function $\Delta\mu^*(T)$ exactly coincides with the slope of the common-tangent at coexistence and in the thermodynamic limit only. Within finite computational cells, $\Delta\mu^*(T)$ is defined even when there is no common tangent, is always easy to determine and fluctuates less than the slope of the common-tangent when there exists one. The transformed Gibbs free energy surfaces $G(c) - c\Delta\mu^*$ are displayed in Fig. 9. The contour plot in the temperature-concentration plane of the bottom panel clearly visualizes the miscibility gap in the composition range going approximately from $\text{Fe}_{0.1}\text{Cr}_{0.9}$ to $\text{Fe}_{0.9}\text{Cr}_{0.1}$.

The coexistence lines (solubility limits) associated with the gap end around 500 K both in the iron-rich or chromium-rich sides and are indicated by the solid white curve in Fig. 9b. Above 525 K, we observe that free energy profiles becomes lower for intermediate composition which indicates the presence of a stability field for these intermediate compositions and of two immiscibility fields for the Fe-rich and Cr-rich compositions. Solubility limits on the Fe-rich and Cr-rich sides associated with the two immiscibility fields are indicated by the dashed white curves in Fig. 9b. However, examination of snapshots of the simulated systems within the expected stability field still shows unmixed microstructures with a tendency to phase separation decreasing with increasing temperature from 525 K to 1700 K. This is attributed to the fact that the correlation length diverges at the critical temperature T_c where the thermodynamic transition is second order. Given that the computational cell contains only 2×6^3 atoms and that atomic interactions up to 7th nearest neighbors were shown to play an important role,³⁶ strong finite-size effects are expected. The low temperature of 500 K measured for the present closure of the miscibility gap should therefore not be interpreted as an estimate of the critical temperature T_c whose experimental value is expected to lie around 900 K.³⁵ A finite-size scaling analysis³⁷ should therefore be carried out, which entails performing simulations with much larger computational cells. To achieve this task, the overall computation time has to be reduced considerably, possibly by evaluating the interatomic potential and forces on parallel computer architectures.³⁸ While the preliminary results presented here show that a direct and accurate construction of the equilibrium phase diagram of FeCr alloy is achievable in principle,

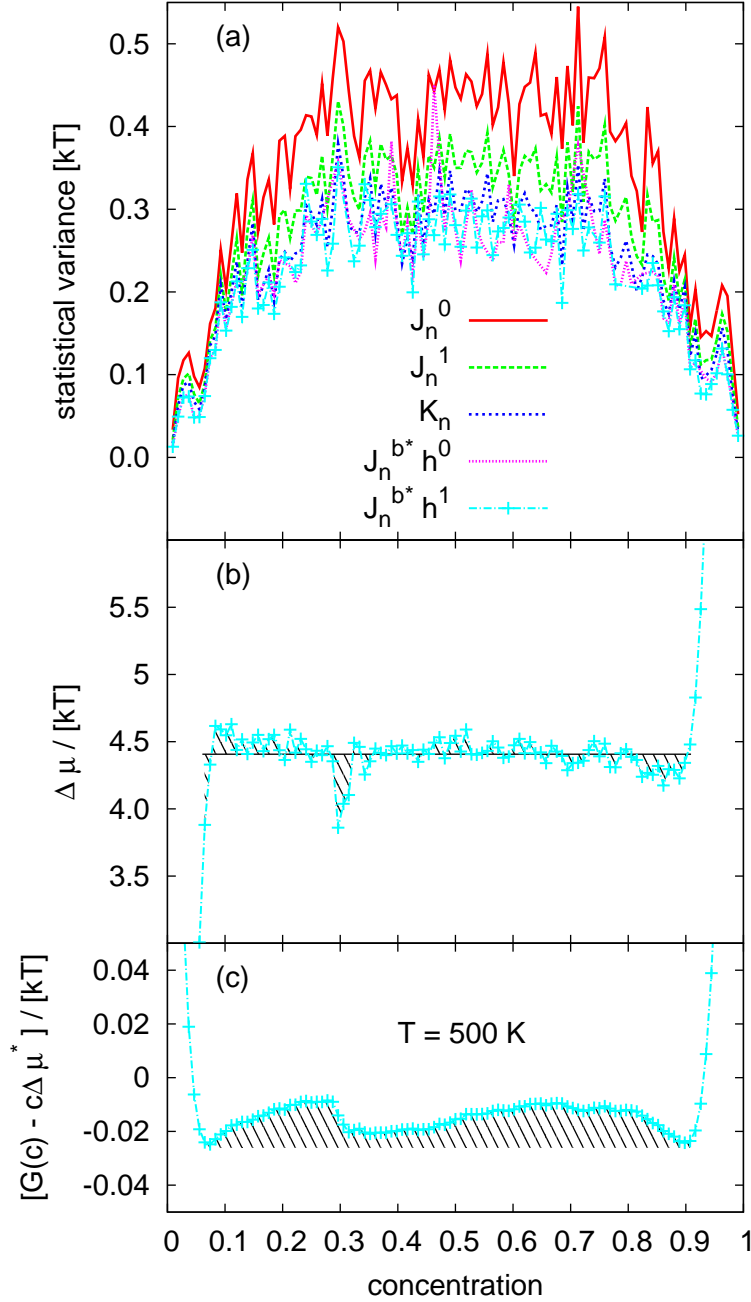


FIG. 8: (a) statistical variances of estimated differences of excess chemical potentials [displayed in (b)];(c) solubility limits displayed in the concentration-temperature plane as obtained from Maxwell equal-area construction at $T = 500$ K. Used estimators are indicated in the legend.

they also emphasize the need for more extensive free energy calculations in this system.

VI. CONCLUDING REMARKS

In this study, the optimal estimator proposed by Delmas and Jourdain for waste-recycling Monte Carlo has been assessed numerically. As a testbed, we implemented the mono-proposal Barker and Metropolis-Hasting algorithms in transmutation ensembles of two alloy systems simulated via the weighted work path ensemble. We simultaneously

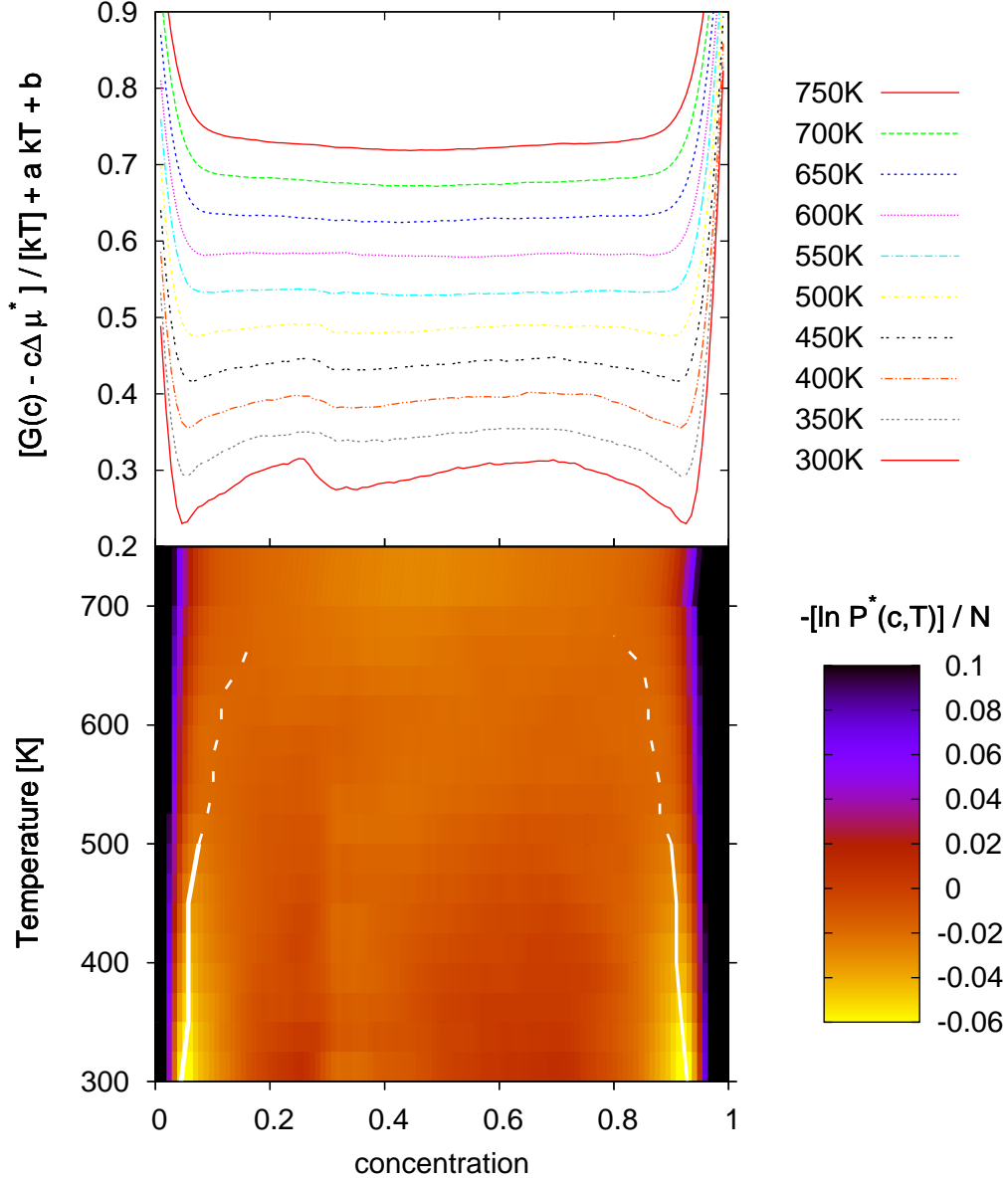


FIG. 9: Top are the Gibbs free energies transformed for better visualization ($a = 10^{-3}$ and $b = \ln Z/N$) as a function of concentration for various temperatures; bright regions on the bottom contour plot correspond to stability fields, the Fe and Cr solubility limits of the Fe-rich and Cr-rich phases are schematized by the two white lines.

estimated the free energy differences from the nonequilibrium works measured along the transmutations. We find that the estimator indeed achieves variance reduction compared to the other Monte Carlo estimators that are compatible with the present sampling approach. Furthermore, the maximal reduction of the statistical variance that is predicted by the theory is attained for relatively short simulations ($2 \cdot 10^3$ sampled paths).

Two other important methodologies have been proposed in the literature for optimally extracting free energy differences from nonequilibrium work measurements. Because they both require implementing specific sampling schemes not suited to the present alloy systems, we did not make any numerical comparisons. The differences in the implementation can nevertheless be emphasized.

The first methodology, proposed by Crooks¹⁷ and extended in Refs. 39 and 40, entails sampling the reference and target thermodynamic states independently while performing bidirectional nonequilibrium work measurements starting from the sampled states. One then resorts to the optimal estimator of Bennett’s acceptance ratio method.⁴¹ A post-processing procedure constructs the optimal estimator from Bayesian inference, neglecting correlations between data.⁴² As the procedure minimizes the variances obtained from a finite sample with respect to some control parameter, the resulting estimator exhibits a statistical bias which becomes negligible only in the limit of large samples, whereas the optimal estimator of Delmas and Jourdain may be stably constructed when not in this limit and is always unbiased.

One limitation of this alternative method relates to the lack of diagnostic tool to check the overlap between the forward and reverse switching processes. Insufficient overlap may result in poorly converged estimates. Another limitation lies in excluding the possibility of swapping between the reference and target states. For instance, when the target state corresponds to a low temperature structure that traps the system in a few basins of attraction, a single simulation of the target system may not fully sample all of these basins.⁴³ Swapping between the reference and target state as employed in this paper can avoid such non-ergodic sampling.

The second methodology^{15,44} entails constructing an optimal biasing distribution rather than optimally post-processing the data obtained in various thermodynamic states. The optimal biasing distribution is derived analytically by minimizing an asymptotic statistical variance given by the central limit theorem.⁴⁵ This approach possesses a number of limitations which we argue that waste recycling on work-weighted transmutation ensembles does not. First of all, the central limit theorem assumes independent and identically distributed random variables while sampled data are inevitably correlated; the denominator of the Delmas-Jourdain control parameter b accounts for these correlations. Secondly, the rejected trial paths are discarded from the optimization procedure, potentially losing valuable information. Thirdly, the shape of the optimal distribution crucially depends on the free energy difference that one wishes to compute and cannot be analytically estimated *a priori*. And finally, the optimal bias distribution constructed in this methodology is bimodal with respect to the work with its two peaks corresponding to the forward and reverse work distributions and with a density depletion in the overlapping region of the two latter distributions. This may result in highly correlated data and poor statistics compared to our work-weighted transmutation ensemble simulations that sample a unimodal distribution exhibiting good overlapping properties in term of work with respect to the distributions obtained with both forward and reverse switching. Overall, we find that the Delmas-Jourdain estimator is unbiased and optimal in terms of asymptotic variance with respect to a simple control variate b^* that can be accurately estimated from the correlations in the collected data. One substantial benefit to employing this optimal estimator is the flexibility in the choice of the sampler, allowing us to couple waste recycling Monte Carlo with a work-weighted transmutation path ensemble ideally formulated to study the phase coexistence of binary alloys. However, in other scenarios, another Monte Carlo sampling scheme might be better posed, yet the optimal estimator of Delmas and Jourdain would still be applied quite similarly. Since information associated with trial switching processes is optimally included in the free-energy estimates for any sampler, this one is to be chosen so as to facilitate the phase space exploration.

Nonetheless, our approach employing the optimal estimator of Delmas and Jourdain shares a qualitative feature with the methodology based on the optimal biasing distribution.⁴⁴ Indeed, forward and reverse trial paths, which contribute substantially to the free energy estimate given by the Delmas-Jourdain estimator for the measured optimal values of the control variate b^* , concomitantly cover the two peaks of the optimal bias distribution.

Concerning the investigated examples of binary alloys, we point out that achieving numerical ergodicity in the reference and target thermodynamic states entails exchanging the allocation of atoms of distinct types on the underlying lattice (which amounts to performing pairs of simultaneous transmutations with opposite direction) with a high enough frequency. With path-sampling, exchanges of atom allocation are automatically achieved when trial paths are successively accepted within the transmutation ensemble (as illustrated in Fig. 1). It turns out that the phase space exploration is considerably facilitated. Resorting to such a path-sampling scheme was found particularly advantageous in the FeCr alloy system which presents a large magnetic misfit. Direct exchange moves sampled using a standard scheme in the reference and target system would have been extremely infrequent and thus computationally expensive compared to the gradual transmutations considered here. The approach might work as well in the numerous alloy systems exhibiting large atomic misfits.

Further assessments of the estimator should consider more general scheduling for the nonequilibrium dynamics rather than simply Eq. (5) and a multi-proposal sampling scheme. Optimal waste-recycling estimators can possibly be derived with multiple proposals based on the same control variate problem structure.¹³ Work in this direction is in progress.³⁸

Acknowledgments

We warmly thank Benjamin Jourdain for suggesting that we test the optimal estimator and for advising us. Stimulating discussions with Berend Smit, Christoph Dellago and Peter Bolhuis are also gratefully acknowledged.

Appendix A: Residence-weight estimator

In the context of path-sampling, waste-recycling estimators may also be derived from statistical inference. The algorithm indeed samples a marginal probability distribution associated with the Bayesian prior P_θ . As a result, information relative to unselected trajectories or to states contained in the trajectories themselves may be inferred online from a Bayesian posterior likelihood without post-processing. The marginal probability density of the sampled web $\{z, \tilde{z}\}$ is

$$\Phi_\theta(\{z, \tilde{z}\}) = \frac{1}{2} [q(\{z, \tilde{z}\} | z) P_\theta(z) + q(\{z, \tilde{z}\} | \tilde{z}) P_\theta(\tilde{z})]. \quad (\text{A1})$$

recalling that q is the conditional probability to construct $\{z, \tilde{z}\}$ from either z or \tilde{z} . The factor $1/2$ acts as a normalizing constant and relates to the position of the prior z in $\{z, \tilde{z}\}$. $P_\theta(z)$ and $P_\theta(\tilde{z})$ are the prior probabilities of $\{z, \tilde{z}\}$.

With the Boltzmann sampler, the rejection probability of \tilde{z} is $1 - p^B(\tilde{z} | \{z, \tilde{z}\})$. It is equal to the posterior likelihood $p^B(z | \{z, \tilde{z}\})$ of z and to the acceptance probability of z constructed from \tilde{z} using the proposal probability $q_\alpha(\{z, \tilde{z}\} | \tilde{z})$. Posterior likelihoods relate to marginal and conditional probabilities via Bayes theorem

$$p^B(z_c | \{z, \tilde{z}\}) = \frac{\frac{1}{2} q(\{z, \tilde{z}\} | z_c) P(z_c)}{\Phi_\theta(\{z, \tilde{z}\})} \quad (\text{A2})$$

where z_c is either z or \tilde{z} . As a result, the Boltzmann sampler leaves invariant the probability distribution $\Phi_\theta(\{z, \tilde{z}\})$, since it satisfies the detailed balance equation ($z_c \in \{z, \tilde{z}\} \cap \{z', \tilde{z}'\}$)

$$q(\{z', \tilde{z}'\} | z_c) p^B(z_c | \{z, \tilde{z}\}) \Phi_\theta(\{z, \tilde{z}\}) = q(\{z, \tilde{z}\} | z_c) p^B(z_c | \{z', \tilde{z}'\}) \Phi_\theta(\{z', \tilde{z}'\}). \quad (\text{A3})$$

In Eq. (A3), both $p^B(z_c | \{z', \tilde{z}'\})$ and $p^B(z_c | \{z, \tilde{z}\})$ correspond to either an acceptance or a rejection probability.

Let Γ_α denote the space of webs sharing a common state at $t = \alpha\tau$. The total web space is $\Gamma_0 \cup \Gamma_1$ and we have equipartition of webs in Γ_0 and Γ_1 . The free energy differences can be cast in the form¹¹ ($\alpha \in \{0, 1\}$)

$$\begin{aligned} e^{g_\theta - g_\alpha} &= \int_{\Gamma_\alpha} q_\alpha(\{z, \tilde{z}\} | z) P_\theta(z) e^{\beta(\theta - \alpha)W(z)} + q_\alpha(\{z, \tilde{z}\} | \tilde{z}) P_\theta(\tilde{z}) e^{\beta(\theta - \alpha)W(\tilde{z})} \mathcal{D}z \mathcal{D}\tilde{z} \\ &= \int_{\Gamma_\alpha} \left[p_\alpha^B(z | \{z, \tilde{z}\}) e^{\beta(\theta - \alpha)W(z)} + p_\alpha^B(\tilde{z} | \{z, \tilde{z}\}) e^{\beta(\theta - \alpha)W(\tilde{z})} \right] \Phi_\theta(\{z, \tilde{z}\}) \mathcal{D}z \mathcal{D}\tilde{z} \\ &= 2 \int_{\Gamma_\alpha} \left[e^{\beta(\alpha - \theta)W(z)} + e^{\beta(\alpha - \theta)W(\tilde{z})} \right]^{-1} \Phi_\theta(\{z, \tilde{z}\}) \mathcal{D}z \mathcal{D}\tilde{z} \end{aligned}$$

Since the algorithm sample the distribution Φ_θ , the free energy difference $g_\theta - g_\alpha$ can be estimated from the logarithm of the following estimator

$$K_n \left(e^{\beta(\theta - \alpha)W} \right) = \frac{4}{n} \sum_{k=1}^{n/2} \left[e^{\beta(\alpha - \theta)W(z_{2k+\alpha})} + e^{\beta(\alpha - \theta)W(\tilde{z}_{2k+\alpha})} \right]^{-1}. \quad (\text{A4})$$

In Eq. (A4), trial paths \tilde{z}_{2k} and \tilde{z}_{2k+1} are generated forward and backward, respectively. Hence, we have $(z_{2k+\alpha}, \tilde{z}_{2k+\alpha}) \in \Gamma_\alpha$. For more details, see Ref. 11.

¹ D. Frenkel, Waste-recycling Monte Carlo, in ‘‘Computer Simulations in Condensed Matter Systems’’, Lect. Notes Phys. **703**, 127 (2006).

² D. Ceperley, G. Ghester and M. Kalos, Phys. Rev. B **16**, 3081 (1977).

³ D. Frenkel, Proc. Natl. Acad. Sci. U.S.A. **101**, 17571 (2004).

⁴ I. Coluzza and D. Frenkel, ChemPhysChem **6** 1779 (2005).

- ⁵ M. Athènes and F. Calvo, *ChemPhysChem* **9**, 2332 (2008).
- ⁶ M Athènes, *Phys. Rev. E*, **66**, 046705 (2002).
- ⁷ M. Athènes, *Eur. Phys. J. B*, **38**, 651 (2004).
- ⁸ M Athènes, *Phys. Rev. E* **66**, 016701 (2002).
- ⁹ G. Boulougouris and D. Frenkel, *J. Chem. Theory Comp.* **1**, 389 (2005).
- ¹⁰ M. Athènes, M.-C. Marinica, *J. Comput. Phys.* **229**, 7129 (2010).
- ¹¹ M. Athènes, *Eur. Phys. J. B*, **58**, 83, (2007).
- ¹² J.-F. Delmas, B. Jourdain, arXiv:math/0611949v1.
- ¹³ J.-F. Delmas, B. Jourdain, *J. Appl. Probab.* **46**, 938 (2009).
- ¹⁴ D. Frenkel and B. Smit, *Understanding molecular simulation*, Academic Press, New York 2002, p389.
- ¹⁵ T. Lelièvre, M. Rousset and G. Stoltz, *Free-energy computations: a mathematical perspective*, Imperial College Press, 2010.
- ¹⁶ G. Crooks, *J. Stat. Phys.* **90**, 1481 (1998).
- ¹⁷ G. Crooks, *Phys. Rev. E* **61**, 2361 (2000).
- ¹⁸ G. Hummer and A Szabo, *Proc. Natl. Acad. Sci. U.S.A.* **98**, 3658 (2001).
- ¹⁹ A. Laio, M. Parrinello, *Proc. Nat. Acad. Sci. USA* **99**, 12562 (2002).
- ²⁰ C. Jarzynski, *Phys. Rev. Lett.* **78**, 2690 (1997).
- ²¹ C. Jarzynski, *Eur. Phys. J. B* **59**, 331 (2008).
- ²² G. Adjanor and M. Athènes, *J. Chem. Phys.* **123**, 234104 (2005).
- ²³ S. X. Sun, *J. Chem. Phys.* **118**, 5769 (2003).
- ²⁴ H. Oberhofer, C. Dellago and P. L. Geissler, *J. Phys. Chem. B* **109**, 6902 (2005).
- ²⁵ W. Lechner and C. Dellago, *J. Stat. Mech.* **04**, P04001 (2007).
- ²⁶ C. Jarzynski, *C. R. Physics* **8**, 495 (2007).
- ²⁷ J. Horowitz and C. Jarzynski, *J. Stat. Mech.: Theory Exp.* **11**, P11002 (2007).
- ²⁸ G N Bochkov and Yu. E. Kuzovlev, *J. Exp. Theor. Phys.* **72**, 238 (1977).
- ²⁹ G N Bochkov and Yu. E Kuzovlev, *Physica A* **106**, 443 (1981).
- ³⁰ F.M. Ytreberg, R.H. Swendsen, D.M. Zuckermann, *J.Chem. Phys.* **125**, 184114 (2006).
- ³¹ M. Duflo. *Random iterative models*, volume 34 of *Applications of Mathematics* (New York). Springer-Verlag, Berlin, 1997.
- ³² F. Ducastelle, *Order and Phase Stability in Alloys*, Elsevier Science Publisher, North Holland, 1991.
- ³³ M. Athènes, P. Bellon and G. Martin, *Acta Mat.* **48**, (2000) 2675.
- ³⁴ P. Olsson, J. Wallenius, C. Domain, K. Nordlund, L. Malerba, *Phys. Rev. B* **72**, 214119 (2005) and *Phys. Rev. B* **74**, 229906 (2006).
- ³⁵ G. Bonny, R. Pasianot, L. Malerba, A. Caro, P. Olsson, M. Yu. Lavrentiev, *J. Nucl. Mater.* **385**, 268 (2009).
- ³⁶ C. Pareige, C. Domain and P. Olsson, *J. Appl. Phys.* **106**, 104906 (2009).
- ³⁷ D. Landau and K. Binder, *A guide to Monte Carlo simulations in Statistical Physics*, Cambridge University Press (2010).
- ³⁸ J. Kim, J. M. Rodgers, M. Athènes, and B. Smit, in preparation.
- ³⁹ P. Maragakis, F. Ritort, C. Bustamante, M. Karplus, and G. Crooks, *J. Comp. Phys.* **129**, 024102 (2008).
- ⁴⁰ D. Minh and A. Adib, *Phys. Rev. Lett.* **100**, 180602 (2008).
- ⁴¹ C. H. Bennett, *J. Comp. Phys.* **22**, 245 (1976).
- ⁴² M. Shirts and J. Chodera, *J. Chem. Phys.* **129**, 124105 (2008).
- ⁴³ G. Adjanor, M. Athènes, and F. Calvo, *Eur. Phys. J. B* **53**, 47 (2006).
- ⁴⁴ H. Oberhofer and C. Dellago, *Comp. Phys. Com.* **179**, 41 (2008).
- ⁴⁵ M.-H. Chen and Q.-M. Shao, *Ann. Stat.* **25**, (1997) 1563.